
Accuracy and Reproducibility of Absolute Quantification of Myocardial Focal Tracer Uptake from Molecularly Targeted SPECT/CT: A Canine Validation

Yi-Hwa Liu, Zakir Sahul, Christopher A. Weyman, Donald P. Dione, Wawrzyniec L. Dobrucki, Choukri Mekkaoui, Matthew P. Brennan, William J. Ryder, and Albert J. Sinusas

Section of Cardiovascular Medicine, Department of Internal Medicine, Yale University School of Medicine, New Haven, Connecticut

Accurate and reproducible SPECT quantification of myocardial molecular processes remains a challenge because of the complication of heterogeneous background and extracardiac activity adjacent to the heart, which causes errors in the estimation of myocardial focal tracer uptake. Our aim in this study was to introduce a heuristic method for the correction of extracardiac activity into SPECT quantification and validate the modified quantification method for accuracy and reproducibility using a canine model. **Methods:** Dual-isotope-targeted ^{99m}Tc and ^{201}Tl perfusion SPECT images were acquired using a hybrid SPECT/CT camera in 6 dogs at 2 wk after myocardial infarction. Images were reconstructed with and without CT-based attenuation correction, and the reconstructed SPECT images were filtered and quantified simultaneously with incorporation of extracardiac radioactivity correction, gaussian fitting, and total-count sampling. Absolute myocardial focal tracer uptake was quantified from SPECT images using 3 different normal limits (maximum entropy [ME], mean-squared-error minimization [MSEM], and global minimum [GM]). SPECT-quantified percentage injected dose (%ID) was calculated and compared with the well-counted radioactivity measured from the postmortem myocardial tissue. SPECT quantitative processing was performed by 2 different individuals with extensive experience in cardiac image processing, to assess reproducibility of the quantitative analysis. **Results:** Correlations between SPECT-quantified and well-counted %IDs using 3 different normal limits were excellent (ME: $r = 0.82$, $y = 0.932x - 0.0102$; MSEM: $r = 0.73$, $y = 1.1413x - 0.0052$; and GM: $r = 0.7$, $y = 1.2147x - 0.0002$). SPECT quantification using ME normal limits resulted in an underestimation of %ID, as compared with well-counted %ID. Myocardial focal tracer uptake quantified from SPECT images without CT-based attenuation correction was significantly lower than that with the attenuation correction. The %IDs quantified from attenuation-corrected SPECT images using MSEM and GM normal limits were not significantly different from well-counted %IDs. Reproducibility of the SPECT quantitative analysis was excellent (ME: $r = 0.98$, $y = 0.9221x + 0.0001$; MSEM: $r = 0.97$, $y = 0.9357x + 0.0004$; and GM: $r = 0.96$, $y = 0.9026x + 0.001$). **Conclusion:** Our SPECT/CT quantification algorithm for the assessment of regional radioactivity may allow for accurate

and reproducible serial noninvasive evaluation of molecularly targeted tracers in the myocardium.

Key Words: SPECT/CT; dual-isotope imaging; hot spot quantification; molecularly targeted cardiac imaging

J Nucl Med 2011; 52:453–460

DOI: 10.2967/jnumed.110.082214

Targeted molecular imaging has the potential of providing invaluable quantitative in vivo information about molecular processes in the heart, such as myocardial angiogenesis (1), apoptosis (2,3), and ventricular remodeling (4,5). Radiolabeled agents targeted at these molecular processes result in focal hot spot images, which are different from the conventional myocardial perfusion images typically acquired that create a cold spot within the heart. The detection of these molecular processes is particularly challenging because the focal or low levels of tracer uptake is associated with the targeted molecular processes in relation to the background activity. The observed uptake within the heart depends on the relative myocardial extraction and specificity of the molecular targeted tracers used and the sensitivity of the imaging system. Accurate and reproducible quantitative assessments of these molecular processes present another challenge because quantification of the target radiotracer within the myocardium is inevitably complicated by the heterogeneous background and extracardiac radioactivity adjacent to the heart, which causes errors in the estimation of myocardial tracer uptake. Recently, our group has focused on the detection, characterization, and measurement of focal myocardial tracer uptake using a dual-isotope SPECT imaging protocol with targeted ^{99m}Tc -labeled hot spot and ^{201}Tl perfusion agents (6,7). We reported previously the first, to our knowledge, hot spot SPECT quantification approach (6) for assessing tracer uptake in the myocardium. This method was validated using a cardiac phantom under ideal conditions in which no background and extracardiac activity were simulated. In this paper, we introduce a heuristic approach into the cardiac SPECT quantification method for the correction of

Received Aug. 12, 2010; revision accepted Dec. 13, 2010.

For correspondence or reprints contact: Yi-Hwa Liu, Section of Cardiovascular Medicine, Department of Internal Medicine, Yale University School of Medicine, New Haven, CT 06520.

E-mail: yi-hwa.liu@yale.edu

COPYRIGHT © 2011 by the Society of Nuclear Medicine, Inc.

extracardiac activity. This modified approach is validated for accuracy and reproducibility using a chronic canine model of myocardial infarction (MI).

MATERIALS AND METHODS

Surgical Preparation

Dogs of either sex ($n = 6$) weighing approximately 25 kg were premedicated with an intravenous injection of thiopental (Pentothal; Abbot Laboratories) (5 mg/kg). The dogs were then intubated and anesthetized with halothane (1%–3%) and nitrous oxide (65%). The dogs were subsequently injected with a slow intravenous loading bolus of amiodarone (30–50 mg), followed by continuous infusion (0.3 mg/min) to prevent lethal arrhythmias. A percutaneous transluminal coronary occlusion was performed via the femoral artery, with a standard over-the-wire balloon angioplasty catheter (diameter, 2–3 mm; length, 10–15 mm). The left anterior descending coronary artery was occluded distal to the first septal perforator for approximately 3 h, resulting in a nontransmural MI. The balloon was deflated and removed, and coronary patency was confirmed by coronary angiography. The femoral site was repaired, and the dogs were allowed to recover from the anesthesia. Aspirin (81 mg) was administered orally for 3 d before angioplasty balloon occlusion, and daily postintervention was performed to prevent coronary thrombosis and ensure coronary patency after reperfusion. The dogs were reanesthetized at 2 wk after MI for in vivo SPECT/CT. All experimental protocols were approved by the Institutional Animal Care and Use Committees at the Yale University School of Medicine according to the guiding principles of the American Physiologic Society on research animal use.

Hybrid SPECT/CT Image Acquisitions and Reconstructions

A dual-head SPECT/CT camera (Infinia; GE Healthcare) equipped with low-energy and high-resolution parallel-hole collimators was used for all image acquisitions. A 15% energy window was centered at 75 keV for the ^{201}Tl photopeak and at 140 keV for the $^{99\text{m}}\text{Tc}$ photopeak for simultaneous dual-isotope SPECT. Some negligible cross-talk contamination between the 2 energy windows using this dual-isotope imaging approach occurred. An external spheric source (diameter, 7.86 mm) filled with $^{99\text{m}}\text{Tc}$ (518–740 kBq [14–20 μCi]) was attached to the dog's chest superior to the heart. The spheric source was used as an external reference for the calculation of absolute tracer uptake in the myocardium. A $^{99\text{m}}\text{Tc}$ -labeled peptidomimetic (RP805; Lantheus Medical Imaging) that targets matrix metalloproteinase activation was injected intravenously into the dogs (740–1,295 MBq [20–35 mCi]). Approximately 4 h after the RP805 injection, ^{201}Tl (74–111 MBq [2–3 mCi]) was injected as a reference agent to define myocardial perfusion. In the context of this report, we refer to the $^{99\text{m}}\text{Tc}$ -labeled RP805 and ^{201}Tl as hot spot and cold spot SPECT radiotracers, respectively. Simultaneous dual-isotope ($^{99\text{m}}\text{Tc}$ -labeled RP805 and ^{201}Tl) SPECT was performed at 15 min after ^{201}Tl injection, using a 360° circular orbit (60 stops/head, 20 s/stop) and 64×64 matrix size (5.4 mm² pixel size). CT images were acquired immediately after dual-isotope SPECT and were reconstructed using conventional filtered backprojection to generate CT attenuation maps. SPECT images were reconstructed with CT-based attenuation correction (AC) and without the attenuation correction (NC) using 2 iterations and 10 subsets of the ordered-

subset expectation and maximization algorithm (8). A 3-dimensional (3D) Butterworth filter with a cutoff frequency of 0.4 cycles/cm and an order of 5 was used to smooth the SPECT images. The final filtered images were reoriented to obtain the short-axis, horizontal long-axis, and vertical long-axis slices of the left ventricle (LV). To ensure precise coregistration between ^{201}Tl perfusion and $^{99\text{m}}\text{Tc}$ -labeled SPECT images, the cold spot and hot spot SPECT images were reconstructed, filtered, and orientated together using a paired processing approach. Figure 1 shows a set of ^{201}Tl cold spot, $^{99\text{m}}\text{Tc}$ hot spot, and fusion SPECT short-axis slices from a representative dog. The ^{201}Tl SPECT slices were coded in green and $^{99\text{m}}\text{Tc}$ SPECT slices were coded in red with a linear color scale. The fusion images illustrate the precise coregistration between the cold spot and hot spot SPECT images that results from the paired processing scheme. Two weeks after MI, an anterior-lateral myocardial perfusion defect (cold spot) can be observed in the ^{201}Tl SPECT images, and focal uptake of the hot spot agent can be seen in the same anatomic region in the $^{99\text{m}}\text{Tc}$ -labeled SPECT images. Under these experimental conditions, and at this time, we observed primarily an inverse relationship between ^{201}Tl perfusion and $^{99\text{m}}\text{Tc}$ -labeled RP805 retention.

Total-Count Data Sampling

The paired processing scheme was embedded in our SPECT quantification algorithm. The numbers of short-axis slices used in the quantification and the final regions of interest were selected on the basis of the ^{201}Tl images. Concordance of the myocardial contours used for the quantitative analysis of both images was confirmed visually by the operator. For finer data sampling, the selected SPECT short-axis slices were interpolated into 36 slices, and each of the interpolated slices was further divided into 128 radial sectors. Consequently, a total-count sampling scheme incorporated with gaussian fitting (6) was used to integrate, on a sector-by-sector basis, the counts (pixel values) within the myocardial contours determined by the gaussian fitting (Supplemental Fig. 3; supplemental materials are available online only at <http://jnm>).

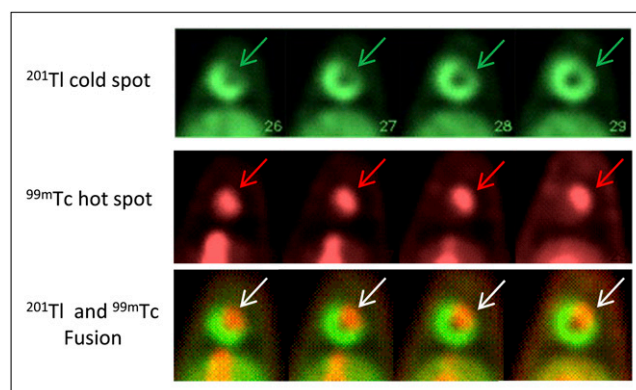


FIGURE 1. Illustration of dual-isotope SPECT short-axis slices from representative dog. ^{201}Tl cold spot SPECT slices were coded in green, and $^{99\text{m}}\text{Tc}$ hot spot SPECT slices were coded in red. Cold spot and hot spot images were subsequently fused as display in third row of panel. Same regions of cold spot (green arrows) and hot spot (red arrows) are shown in anterior-lateral wall of LV, demonstrating excellent coregistration and approximately reciprocal relationship between cold spot and hot spot SPECT images (white arrows).

snmjournals.org). The total-count sampling approach was also applied to the external spheric source modeled as 3D gaussian (6). This total-count sampling scheme was designed to minimize the partial-volume effect of SPECT (9,10). To facilitate comparison with the postmortem data, the total number of slices, anatomic regions, and orientation of the SPECT slices were selected to correspond with the postmortem myocardial slices.

Extracardiac Activity Correction

Radioactivity from extracardiac organs, such as the liver, inevitably causes an error in the estimation of regional myocardial tracer uptake. This extracardiac count spillover is in part due to the limited SPECT resolution and needs to be corrected in the total-count sampling. The extracardiac activity generally appears in the regions adjacent to the inferior wall of the LV. As such, prior information for true cardiac activity (not contaminated by the extracardiac organ) can be obtained from the anterior regions of the LV. Our algorithm (7) for the extracardiac activity correction is in part derived from these observations, and derivations of this algorithm are described in the supplemental data.

The total-count sampling process was further tailored and refined with the incorporation of the extracardiac activity correction (supplemental data). The total counts of each myocardial sector derived from ^{99m}Tc -labeled hot spot SPECT were normalized to the total counts of the external spheric source (6), whereas the total counts derived from ^{201}Tl cold spot SPECT were normalized to the peak value of the entire LV (i.e., global normalization). As a result, 36 circumferential count profiles, each with 128 myocardial sectors, were generated from the short-axis slices of hot spot and cold spot SPECT images.

Normal Limits of Myocardial Focal Tracer Uptake

To calculate abnormal myocardial focal tracer uptake, a normal limit needs to be predetermined. In this experimental validation, we used 3 approaches to estimate the normal hot spot limit. Of those, 1 was derived from the maximum entropy (ME) of ^{201}Tl myocardial perfusion and ^{99m}Tc -labeled hot spot SPECT images, with the assumption that there existed an approximately reciprocal relationship between the regional intensity of these cold spot and hot spot imaging agents (6), as illustrated in Figure 1. More specifically, the estimation procedure was considered a stochastic process (11–13). The ME of the count profiles derived from the ^{201}Tl myocardial perfusion and ^{99m}Tc -labeled hot spot SPECT images was calculated and subsequently maximized by a line-search algorithm (6) to obtain an optimal hot spot normal limit based on the ME principle. However, depending on the radiotracers used and the experimental conditions, a reciprocal relationship may not always exist. Thus, we introduce 2 additional approaches for the estimation of normal hot spot limits: one based on the concept of mean-squared-error minimization (MSEM) (11), and the other based on the global minimization (GM) of hot spot circumferential count profiles. More specifically, the MSEM normal hot spot limit was calculated by the mean of minimums over the entire hot spot circumferential count profiles as

$$T = \frac{1}{N} \sum_{s=1}^N \min_{\theta} [\zeta(\theta, s)], \quad \text{Eq. 1}$$

and the GM normal hot spot limit was determined by the minimum of minimums over the entire circumferential hot spot count profiles as

$$T = \min_s \{ \min_{\theta} [\zeta(\theta, s)] \}, \quad \text{Eq. 2}$$

where $\zeta(\theta, s)$ represents the normalized total counts of radial sector θ in SPECT slice s , and N denotes the total numbers of slices included in the quantification. Notice that unlike the ME approach, the latter 2 estimation approaches (MSEM and GM) do not need the perfusion cold spot SPECT as a reference to estimate the normal hot spot limit.

Calculation of Myocardial Focal Tracer Uptake

Hot spot circumferential count profiles were compared with the normal hot spot limits to calculate focal tracer uptake in the myocardium. Myocardial radial sectors with focal tracer uptake greater than the normal limit were considered as abnormal, and the absolute focal tracer uptake from the abnormal myocardial sectors was then calculated as the difference between hot spot circumferential count profiles and the normal limit as

$$\text{Total hot spot uptake} = d \times \sum_s [w(s) \times \sum_{\theta} (\zeta(\theta, s) - T)], \quad \text{Eq. 3}$$

where d denotes the known dose in the external spheric source, $w(s)$ is the volume-weighting factor for slice s , and T is the predetermined normal hot spot limit. Alternatively, the myocardial hot spot uptake can be expressed as percentage of injected dose (%ID) by dividing the absolute hot spot uptake by the total dose of hot spot radiotracer injected as

$$\%ID = \frac{\text{Total hot spot uptake}}{\text{Injected dose}} \times 100. \quad \text{Eq. 4}$$

Radioactivity Measurements from Postmortem Myocardial Tissue

After SPECT/CT, dogs were euthanized with an intravenous injection of potassium chloride, and the hearts were extracted and washed with normal saline. The hearts were filled with dental molding material (alginate impression material, type II, normal set; Quala Dental Products) by retrograde infusion through the pulmonary artery and aorta, to facilitate myocardial tissue cutting. The LV was isolated and cut into approximately 5-mm-thick short-axis slices starting from just below the membranous septum down to the apex. Each of these postmortem myocardial slices was further divided into 16 radial sectors for γ -well counting of ^{99m}Tc radioactivity. The well-counted radioactivity was subsequently corrected for background activity, spill-up, spill-down, and radioactive decay.

Accuracy Assessment

SPECT-quantified and well-counting data were interpolated into 12 composite myocardial sectors (3 short slices [apical, mid ventricle, and basal] \times 4 radial sectors [anterior, septal, inferior, and lateral]) for each dog. Myocardial activity (%ID) derived from quantification of the SPECT images was compared with the activity (%ID) derived from γ -well counting on a sector-by-sector basis to assess the accuracy of SPECT hot spot quantification. As a result, 12×6 ($n = 72$) composite myocardial sectors for 6 dogs were compared in this study.

Reproducibility Assessment

The procedures of SPECT processing and quantitative data analysis described herein were performed by 2 different operators to assess the reproducibility of our SPECT quantitative analyses.

To retain independence between the 2 operators, the individuals were trained initially for the entire processing procedures but were not re-instructed afterward. Interoperator reproducibility was assessed by correlation and mean difference between the SPECT results obtained from the 2 operators.

Statistical Analysis

Linear regression and Bland–Altman (14) analyses were used in our comparisons of data derived from SPECT analyses and γ -well counting. A Student 2-tailed *t* test was used to evaluate differences between 2 measurements. A *P* value of less than 0.05 was considered statistically significant for the comparisons.

RESULTS

Demonstration of Performance of Extracardiac Activity Correction

Figure 2 shows a pair of coregistered ^{201}Tl perfusion (2A) and $^{99\text{m}}\text{Tc}$ -labeled RP805 (2B) SPECT short-axis slices and the corresponding circumferential count profiles (2C and 2D) from a representative dog used in this study. The ^{201}Tl circumferential count profiles (yellow curves in Figs. 2C and 2D) are similar, whereas the hot spot $^{99\text{m}}\text{Tc}$ count profile (red curve in Fig. 2C) being generated without the extracardiac activity correction shows an erroneous peak of hot spot uptake (red arrow in Fig. 2C) in the inferior region of the LV, presumably caused by the count spillover from the liver (Fig. 2B). The erroneous hot spot count profile was improved with the extracardiac activity correc-

tion (red curve in Fig. 2D). Figures 2E and 2F show the correlations between well-counted %ID and SPECT-quantified %ID, without and with the extracardiac activity correction, respectively. As seen in Figure 2E, there was no correlation ($r = 0.05$; $y = -0.0376x + 0.0075$) between the 2 assessments when extracardiac activity correction was not applied, whereas the correlation was markedly improved ($r = 0.97$; $y = 0.247x - 0.009$) with the correction (Fig. 2F), demonstrating the importance of the extracardiac activity correction for hot spot quantification. However, there was a systematic underestimation in the assessment of %ID as shown in Figure 2F according to the slope of the regression line, which was less than 1. This underestimation was due to the fact that the CT-based AC had not been applied to the images shown in Figure 2. These results were consistent with our previous phantom study (6) in which we demonstrated the necessity of SPECT/AC for precise absolute quantification of myocardial focal tracer uptake. Consequently, the results were all processed with the corrections of extracardiac activity and photon attenuation.

Accuracy of Hot Spot SPECT Quantification

Figure 3 shows the scatterplots for comparisons between well-counted %IDs and SPECT-quantified %IDs using 3 normal hot spot limits (ME, MSEM, and GM). As seen, well-counted %IDs correlated quite well with SPECT-quantified %IDs for all 3 normal hot spot limits (ME: $r = 0.82$, $y =$

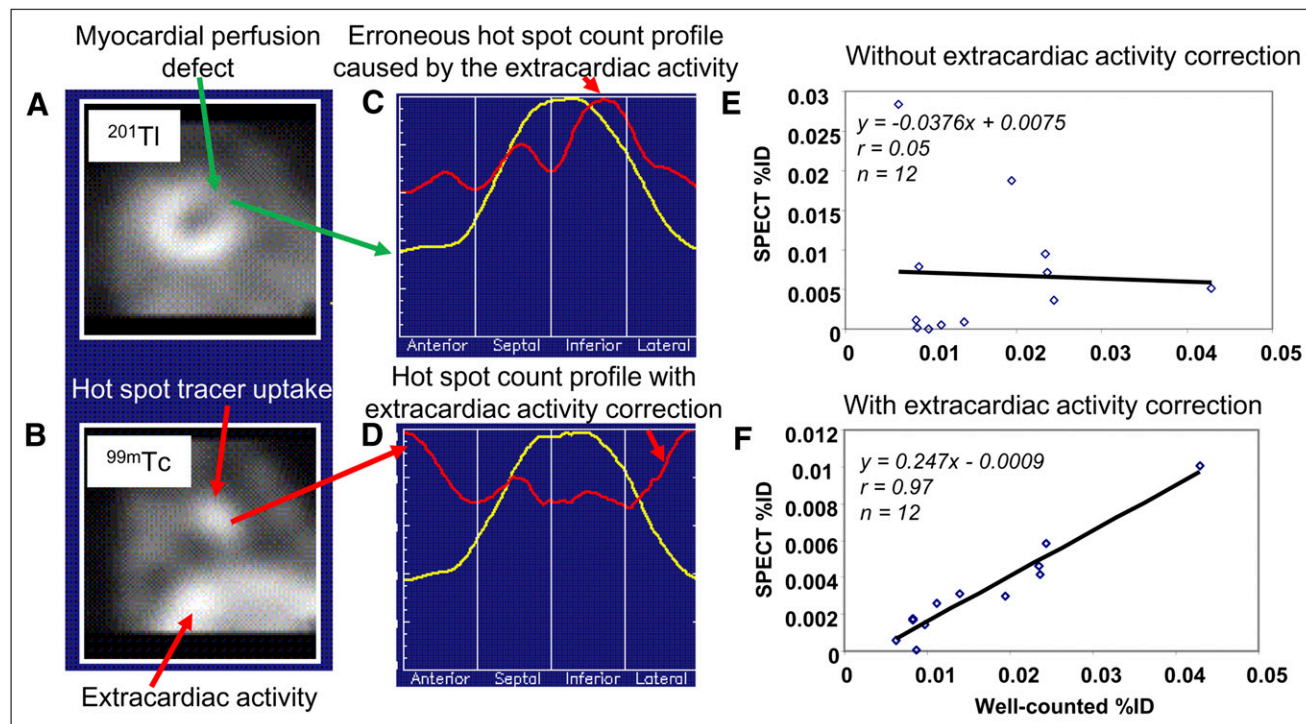


FIGURE 2. Illustration of in vivo SPECT short-axis slices, circumferential count profiles, and sector-by-sector comparisons of SPECT-quantified vs. well-counted myocardial hot spot tracer uptake from representative dog. (A) ^{201}Tl perfusion SPECT short-axis slice. (B) $^{99\text{m}}\text{Tc}$ -labeled RP805 SPECT short-axis slice. (C and D) Corresponding circumferential count profiles (^{201}Tl in yellow and $^{99\text{m}}\text{Tc}$ in red) of A and B without and with correction of extracardiac activity spillover from liver, respectively. (E and F) Correlations between well-counted %ID and SPECT-quantified %ID from same dog without and with extracardiac activity correction, respectively.

0.932x - 0.0102; MSEM: $r = 0.73$, $y = 1.1413x - 0.0052$; and GM: $r = 0.7$, $y = 1.2147x - 0.0002$). Of those, the ME normal limit resulted in the best correlation ($r = 0.82$). The Bland–Altman analyses of agreement for these comparisons are shown in Supplemental Figure 1. There was a systematic underestimation (Supplemental Fig. 1A) when the ME normal limit was used in the hot spot quantification (mean error, -0.011 ± 0.0069 %ID). This underestimation was expected because there was no normal hot spot limit being incorporated into the well-counting measurements. Namely, entire myocardial sectors from which the hot spot radioactivity was measured were considered abnormal in our well-counting measurements. However, the underestimation was improved (Supplemental Fig. 1B) when the MSEM normal limit was used in the hot spot quantification (mean error, -0.0028 ± 0.011 %ID). The %ID was slightly overestimated (Supplemental Fig. 1C) when the GM normal limit was used in the quantification (mean error, 0.004 ± 0.01 %ID). This overestimation may be attributable to the random background noise being included in the abnormal hot spot uptake calculation using the GM normal limit.

Overall comparisons among entire regional myocardial radioactivity being expressed as mean %ID are shown in Figure 4. As expected, %IDs quantified from the SPECT/NC images were significantly lower than those from the SPECT/AC images, regardless of which normal hot spot limit was used in the quantification ($P < 0.01$). SPECT-quantified %IDs, as compared with the well-counted %IDs (except those quantified from the SPECT/AC images with MSEM and GM normal hot spot limits), were significantly underestimated ($P < 0.01$). More specifically, the SPECT/AC-quantified %IDs were similar to the well-counted %IDs ($P =$ not significant) when the MSEM or GM normal hot spot limits were incorporated into our hot spot quantification.

Reproducibility of Hot Spot SPECT Quantification

Figure 5 shows the scatterplots for the assessments of interoperator reproducibility of SPECT/AC-quantified %IDs. The interoperator reproducibility using 3 different normal hot spot limits was excellent (ME: $r = 0.98$, $y = 0.9221x + 0.0001$; MSEM: $r = 0.97$, $y = 0.9357x + 0.0004$; and GM: $r = 0.96$, $y = 0.9026x + 0.001$). The Bland–Altman

analyses of agreement for these comparisons are shown in Supplemental Figure 2. Mean differences (mean \pm SD) between %IDs obtained from 2 different operators were small (ME, 0.00035 ± 0.0024 %ID; MSEM, 0.00058 ± 0.0042 %ID; and GM, 0.001 ± 0.0049 %ID), regardless of which normal hot spot limit was used in the quantification. Nevertheless, the ME normal limit resulted in the highest agreement ($r = 0.98$) and the smallest difference (mean difference, 0.00035 ± 0.0024 %ID).

DISCUSSION

We have presented a hot spot SPECT quantification method that incorporates extracardiac activity correction and 3 normal hot spot limits for the assessment of regional focal tracer uptake in the myocardium. We validated this modified method using a chronic canine model of MI and demonstrated that the method provided high accuracy and excellent reproducibility in the assessment of absolute myocardial focal radiotracer uptake.

Merits of Dual-Isotope SPECT

The ^{99m}Tc -labeled hot spot agent used in this study was specifically targeted at matrix metalloproteinase activation, a biomarker of left ventricular remodeling (15–17). Dual-isotope (^{201}Tl myocardial perfusion and ^{99m}Tc -labeled hot spot) SPECT/CT images were acquired at approximately 4 h after the injection of ^{99m}Tc -labeled RP805 radiotracer. The 4-h delay for hot spot imaging was determined empirically from our previous finding that myocardial retention of this molecular targeted radiotracer relative to blood clearance was optimal at 2–4 h after the tracer injection. ^{201}Tl perfusion SPECT images being coregistered with hot spot SPECT images were used to provide the anatomic information about the LV. In this study, we found that the ^{201}Tl SPECT images were helpful for the determination of the integral ranges used in our total-count sampling and were also useful for the estimation of the normal hot spot limit based on the joint ME (6). Additionally, the precise image coregistration allowed for the paired processing of cold spot and hot spot SPECT images and also facilitated our fusion image display for the demonstration of the approximately reciprocal relationship between the cold spot and hot spot images at this experimental time point.

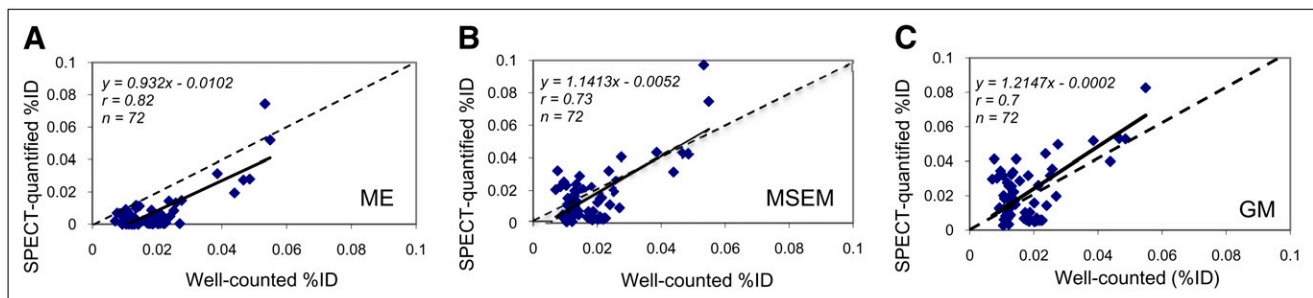


FIGURE 3. Correlations between well-counted %IDs and SPECT %IDs quantified using ME (A), MSEM (B), and GM (C) normal limits. — = line of identity.

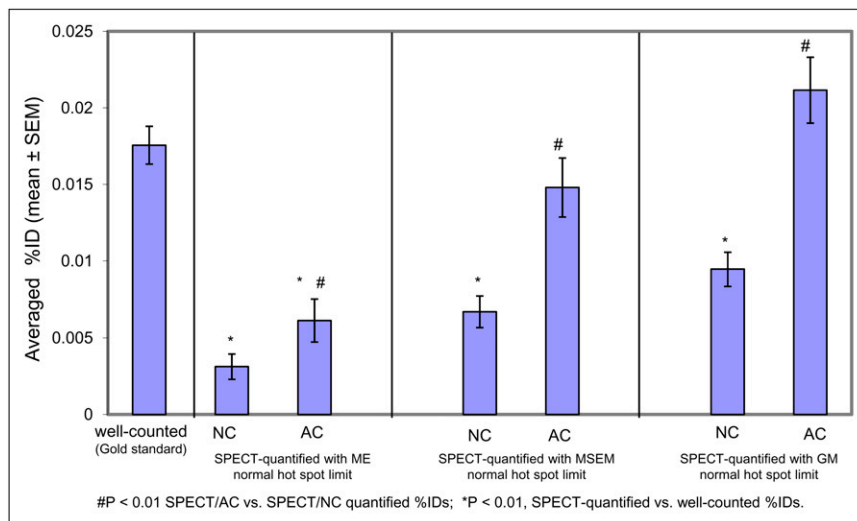


FIGURE 4. Overall comparisons among mean %IDs measured by well-counting and mean %IDs quantified from SPECT/AC and SPECT/NC using 3 different normal hot spot limits.

Extracardiac Activity Correction Incorporated with Gaussian Probability Function

The heuristic approach for the extracardiac activity correction introduced herein was attempted not to correct for the cross-talk between the 2 energy windows used in our dual-isotope SPECT study but to correct for the extracardiac count spillover into the heart. This method appeared to work reasonably well in this canine study for the detection of extracardiac regions and for the correction of the count spillover from the liver. In particular, the count spillover was attributable to the limited SPECT resolution, which can be characterized by the full width at half maximum (FWHM) or SD of the point spread function of the SPECT systems used. The point spread function generally follows the gaussian statistics. As such, the probability density function used in our extracardiac activity correction was derived from the gaussian distribution of which the FWHM or SD was determined by the external spheric source (6,7). The simultaneous SPECT acquisition, reconstruction, and AC for the heart and external spheric source are important, particularly for the extracardiac activity correction incorporated with the gaussian probability function. The parameter (FWHM or SD) of the gaussian function used in our extracardiac activity correction algorithm was not arbitrarily chosen but was derived from the known

external spheric source. The gaussian probability function with the known SD derived from the external spheric source may be more rational and, thus, should work better than other ad hoc linear, quadratic, exponential, and logarithmic functions, for which the parameter values are generally chosen arbitrarily.

Selection of Normal Hot Spot Limits for SPECT Hot Spot Quantification

We have introduced 3 approaches for the estimation of normal hot spot limits in this report: ME, MSEM, and GM. The ME approach was based on our observation of the approximately reciprocal relationship between ²⁰¹Tl cold spot and ^{99m}Tc-labeled hot spot images (i.e., low image intensity in cold spot images would reflect high image intensity in the corresponding hot spot images; Fig. 1). The maximization of the ME of cold spot and hot spot SPECT images for the estimation of normal hot spot limit was designed to increase the dispersion (12,13) of the reciprocal relationship between the cold spot and hot spot SPECT images. In this canine study, we found that our hot spot SPECT quantification algorithm incorporated with the dual-isotope imaging protocol and the ME normal limit worked quite well, as demonstrated in Figures 3 and 5. When compared with the MSEM and GM normal limits,

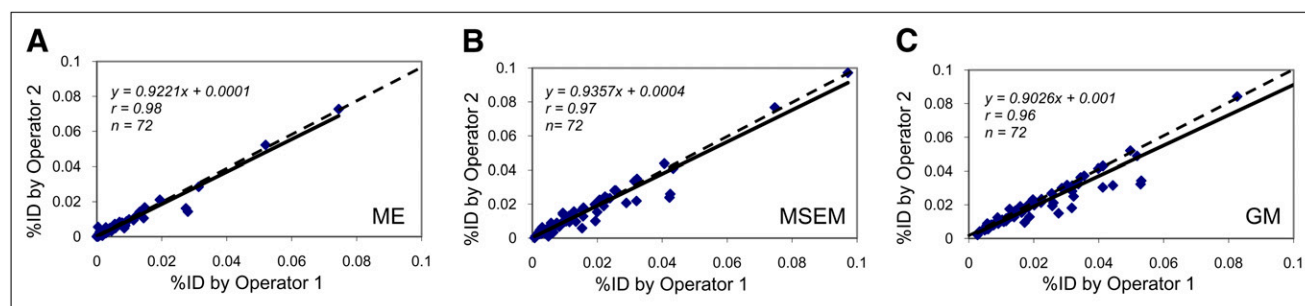


FIGURE 5. Interoperator reproducibility of SPECT-quantified %IDs using ME (A), MSEM (B), and GM (C) normal limits. — = line of identity.

the ME normal limit resulted in the highest correlation coefficients both in the accuracy ($r = 0.82$, Fig. 3A) and in the reproducibility ($r = 0.98$, Fig. 5A) appraisals, although %ID was underestimated (Fig. 4) using the ME normal limit. As mentioned earlier, this underestimation was due in part to the fact that there was no normal limit applied to the well-counting %ID calculations and potential tracer uptake in the normal remote regions. Nonetheless, we believe that the dual-isotope SPECT strategy and ME normal limit introduced here may have merits of accurate and reproducible estimation of absolute focal hot spot tracer in the myocardium under the condition that an approximately reciprocal relationship between the cold spot and hot spot SPECT images exists (6).

The MSEM normal limit was based on the stochastic estimation theory (11,13) in which no a priori was assumed in the data. The GM normal limit, on the other hand, was calculated by the minimal hot spot uptake over the entire LV, representing the most normal hot spot uptake in the LV. In theory, the normal myocardium should have no hot spot uptake in the normal regions, whereas in reality this assumption would not be true because of several confounding variables such as diffuse uptake in the normal myocardium, photon scatter, and background activity. Although the use of a GM normal limit may not be practical for the hot spot quantification from in vivo SPECT images, we calculated this normal limit for the purpose of an additional comparison of SPECT-quantified %ID with the well-counted %ID. We expected that the SPECT-quantified %ID using the GM normal limit should have correlated the best with the well-counted %ID because the normal limits used in these %ID calculations were similar (0 for well-counting and minimal background for SPECT). However, as seen in Figure 3, the %ID was somewhat overestimated when the GM normal limit was used. This overestimation was presumably due to the background noise and photon scatter from the ^{201}Tl energy window into the $^{99\text{m}}\text{Tc}$ window. Although the accuracies of hot spot SPECT quantification using the MSEM and GM normal limits were similar (Fig. 4), the MSEM normal limit may be preferred because hot spot SPECT quantification with the GM normal limit is susceptible to random background noise and photon scatter. Furthermore, the MSEM approach may be useful for the evaluation of some targeted tracers demonstrating focal hot spot uptake in the infarcted myocardium and alterations in absolute uptake in the remote normal myocardium. The effectiveness of the MSEM method is particularly true in the evaluation of post-MI remodeling, which is known to occur in all regions of the myocardium.

Ultimately, the decision on whether the ME or MSEM normal hot spot limit should be used for patients may depend on the characteristics of the hot spot radiotracers used. The preferred method for hot spot SPECT quantification of any given targeted radiotracer may also depend on the anticipated distribution of the radiotracer within the myocardium. More specifically, for tracers only localized

within the MI regions the ME approach may be preferred, whereas if the tracer is also targeted at non-MI regions the MSEM approach may be preferred.

Study Limitations and Future Directions

Cross-talk contamination between the ^{201}Tl and $^{99\text{m}}\text{Tc}$ energy windows presents a potential problem for dual-isotope SPECT with current sodium iodide detectors, for which the energy resolution is known to be suboptimal. However, the cross-talk issue can be addressed by newer technology with solid-state (such as cadmium zinc telluride) detectors, which have better energy resolution than sodium iodide detectors. Another feasible solution to the cross-talk contamination can be the use of CT images in place of ^{201}Tl images to provide the LV anatomic information for the assessment of focal myocardial tracer uptake. In this study, we used CT images only for SPECT/AC because the resolution of the nondiagnostic CT we used in this study was not adequate to differentiate the myocardial borders. However, as 64-slice CT becomes more available, high-resolution CT images can be adapted into our algorithms for the detection of LV contours and the estimation of MSEM and GM normal hot spot limits. In the future, we expect to take advantage of this high-resolution CT to facilitate myocardial edge detection, 3D data sampling, and MSEM and GM normal limit estimation.

CONCLUSION

Our SPECT/CT quantification algorithm for the assessment of regional radioactivity may allow for accurate and reproducible serial noninvasive evaluation of molecularly targeted tracers in the myocardium. The selection of normal hot spot limits for the SPECT quantification of absolute myocardial tracer uptake may be determined by the characteristics of the radiotracers used.

ACKNOWLEDGMENTS

We thank Xiaoyue Hu and Christi Hawley for their assistance in surgical preparation, animal care, and data collection for the entire animal imaging experiments. This work was supported in part by the American Heart Association Grant-in-Aid 0555808T and the National Institutes of Health research grants 1R21 EB001774-01 and 5R01 HL078650-02. The $^{99\text{m}}\text{Tc}$ -labeled RP805 tracer was provided by Lantheus Medical Imaging, North Billerica, MA.

REFERENCES

1. Okada RD, Johnson G, 3rd, Nguyen KN, et al. $^{99\text{m}}\text{Tc}$ -HL91: "hot spot" detection of ischemic myocardium in vivo by gamma camera imaging. *Circulation*. 1998;97:2557-2566.
2. Kang PM, Haunstetter A, Aoki H, Usheva A, Izumo S. Morphological and molecular characterization of adult cardiomyocyte apoptosis during hypoxia and reoxygenation. *Circ Res*. 2000;87:118-125.
3. Kown MH, Steenhoven TV, Blankenberg FG, et al. Zinc-mediated reduction of apoptosis in cardiac allografts. *Circulation*. 2000;102(19, suppl 3):III-228-III-232.

4. Spinale F. Matrix metalloproteinases; regulation and dysregulation in the failing heart. *Circ Res.* 2002;90:520–530.
5. Spinale F, Coker M, Heung L, et al. A matrix metalloproteinase induction/activation system exists in the human left ventricular myocardium and is upregulated in heart failure. *Circulation.* 2000;102:1944–1949.
6. Liu Y-H, Fernando G, Sinusas A. A new method for hot-spot quantification of hybrid SPECT/CT cardiac images: methodology and preliminary phantom validation. *IEEE Trans Nucl Sci.* 2006;53:2814–2821.
7. Liu Y-H, Sahul Z, Weyman C, et al. Hotspot quantification of myocardial focal tracer uptake from molecular targeted SPECT/CT images: experimental validation. *Proc SPIE.* 2008;6915:69150N.1–69150N.8.
8. Hudson HM, Larkin RS. Accelerated image reconstruction using ordered subsets of projection data. *IEEE Trans Med Imaging.* 1994;13:601–609.
9. King MA, Long DT, Brill AB. SPECT volume quantitation: influence of spatial resolution, source size and shape, and voxel size. *Med Phys.* 1991;18:1016–1024.
10. Kojima A, Matsumoto M, Takahashi M, Hirota Y, Yoshida H. Effect of spatial resolution on SPECT quantification values. *J Nucl Med.* 1989;30:508–514.
11. DeGroot M. *Probability and Statistics.* 2nd ed. Reading, MA: Addison-Wesley Publishing Company; 1986.
12. Gallager R. *Information Theory and Reliable Communication.* New York, NY: Wiley; 1968.
13. Van Trees H. *Detection, Estimation, and Modulation Theory.* Vol. I. New York, NY: John Wiley & Son, Inc.; 2001.
14. Bland JM, Altman DG. Statistical methods for assessing agreement between two methods of clinical measurement. *Lancet.* 1986;i:307–310.
15. Thomas CV, Coker ML, Zellner J, Handy J, Crumbley A 3rd, Spinale F. Increased matrix metalloproteinase activity and selective upregulation in LV myocardium from patients with end-stage dilated cardiomyopathy. *Circulation.* 1998;97:1708–1715.
16. Su H, Spinale F, Dobrucki LW, et al. Non-invasive targeted imaging of matrix metalloproteinase activation in a murine model of post-infarct remodeling. *Circulation.* 2005;112:3157–3167.
17. Kramer CM, Sinusas AJ, Sosnovik DE, French BA, Bengel FM. Multimodality imaging of myocardial injury and remodeling. *J Nucl Med.* 2010;51(suppl 1): 107S–121S.